PIV FLOW MEASUREMENTS ON A HIGH LIFT AIRFOIL WITH LEADING EDGE ICE

Joop H.M. Gooden
National Aerospace Laboratory NLR, The Netherlands

Keywords: *icing, performance, airfoil, wind tunnel, flight safety*

Abstract

The aircraft performance decrease due to icing on a wing is an important area of concern for flight safety. A wind tunnel data base has been established for a high lift airfoil with a single flap extended, representative for a modern airliner wing. The model airfoil is equipped with a leading edge ice shape.

This paper presents flow quantities measured by means of the PIV measurement technique on the airfoil upper surface over almost the full wing chord at several angles of attack in the range from pre-stall to post-stall: 0.5°, 3.5°, 4.5°, 5.5°, 6.5° and 8.5°. The flow field was measured by three cameras synchronously, enabling to get snapshots of the full upper surface flow at once. Mean flow as well as turbulence data are presented.

1 Introduction

The prediction of the effect of icing on aircraft performance degradation (and thus flight safety) by means of CFD presently is still very challenging due to the massive flow separations behind the ice shapes on the wing and tail surfaces. Therefore execution of wind tunnel experiments is required to enhance the knowledge of the complex flow behaviour and support computations by providing validation data. But also the proper execution of wind tunnel tests is a challenge since easily unwanted flow instabilities and 3D flow features on a 2D wind tunnel model can occur at incidences around maximum lift and beyond. Traditionally during this type of icing related wind tunnel experiments, general airfoil characteristics like pressure distributions, lift and drag are measured. The unique feature of the subject test campaign, was the measurement of the flow field off the surface of the airfoil. Particle Image Velocimetry (PIV) was used for this purpose. On one hand this gives more insight into the physics of the separated flow behind the ice shape. On the other hand the need was felt to generate more data to validate and improve the capabilities of CFD methods to tackle these kind of flows. The PIV measurements were performed by the Duits-Nederlandse Windtunnels (DNW) in the DNW-LST at NLR-NOP. The test was done in the framework of the Group for Aeronautical Research and Technology in EURope (GARTEUR) Action Group AD(AG40): 'Ice Shape Effects on the Aerodynamic Performance of Aerofoils'.

The test discussed in this paper considers a high lift airfoil, representative of an outboard wing section of a commercial airliner (figure 1). The leading edge ice shape corresponds to an intermediate type of ice between glace and rime ice and was determined in the past from calculation.
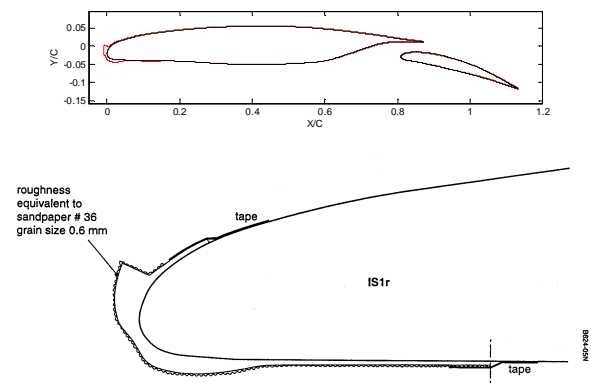

Fig. 1. Airfoil and ice shape

Earlier test results on this airfoil (wing characteristics on the clean airfoil and the airfoil equipped with several ice shapes both with and without flap extended) are reported in [1]. Figure 2 gives the clean and iced $C_l - \alpha$ curves as reported in that reference, showing the serious effect of icing on the performance. Without icing $C_{l,max}$ occurs at $\alpha=12°$. With ice this value drops to 5.5°.
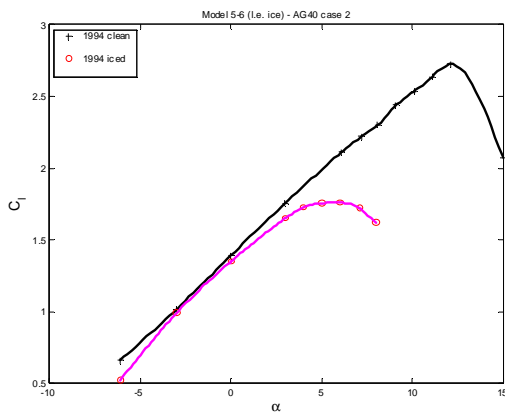

Fig. 2. Lift-coefficient clean and with ice [1]

The present test contained a repeat measurement of the pressure distributions, to allow comparison with the 1994 data. Besides, the flow field on the airfoil upper surface over almost the full wing chord was measured by PIV at several angles of attack in the range from pre-stall to post-stall: 0.5°, 3.5°, 4.5°, 5.5°, 6.5° and 8.5°. At each angle of attack 1000 images of the full upper surface flow were taken by three PIV cameras simultaneously, enabling to get mean flow field characteristics and a good impression of turbulence levels.

2 Test Set-up

2.1 Wind tunnel

The tests were carried out in the DNW-LST in April 2005. The DNW-LST operates at atmospheric conditions and is of the closed return type. The test section is 3 m wide and 2.25 m high with a maximum attainable speed of about 80 m/s. The wind tunnel has an excellent flow quality: flow speed variation is

within 0.2% across the test section. The turbulence levels are extremely low, typically around 0.03%.

2.2 Model

The model used for the test is known as model 5-6. This model represents an outer wing section of a transport aircraft. The shape with extended flap is shown in figure 1. This figure also shows the location of the (X,Y)-coordinate system being used. X=0 corresponds to the clean airfoil leading edge. The main airfoil model characteristics are: chord C=0.6759 m, airfoil thickness t/C=10.6 % and flap deflection δ_f=18°. The model is mounted vertically between the upper and lower turn table in the test section. The flap is mounted using slender brackets on the lower side of the model (figure 3).

Pressure taps with a diameter of 0.8 mm are present in one section 65 mm above the model centre section. Of these, 49 pressures are located in the main wing and 21 in the flap.

To improve two-dimensionality of the flow on 2D models, blowing slots are applied in the turntables a short distance upstream of the wing leading edges (the orange objects on the wind tunnel floor and ceiling in front of the leading edge in figure 3). The pressure ratio equaled 1.7 and was determined from flow visualization tests to optimize flow 2-dimensionality at incidences around maximum lift.
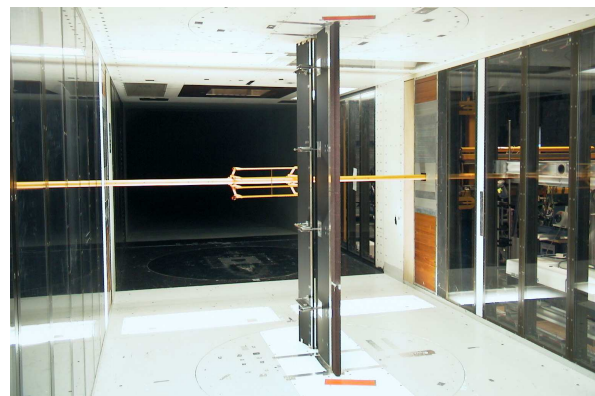

Fig. 3. Model in the DNW-LST

The glaze ice shape was represented by means of cast resin parts attached to the model leading edge. The ice shape extends from 15

%C on the pressure side to 3 %C on the suction side (see also figure 1). The surface of the glace ice shape was made rough by covering the ice shape with sandpaper # 36, having an average grain size of 0.6 mm (figure 4). Ice simulation was applied over the full span except for a part of the leading edge 0.05 m wide at both wing ends to reduce flow separation at the tunnel wall junction. Also a strip of 2 mm width at the pressure tap section was left free, to allow rough pressure distribution measurements in the leading edge area. It is clear that the pressures measured here do not represent accurately the pressure distribution over the ice shape. The ice shape itself was not equipped with pressure taps.
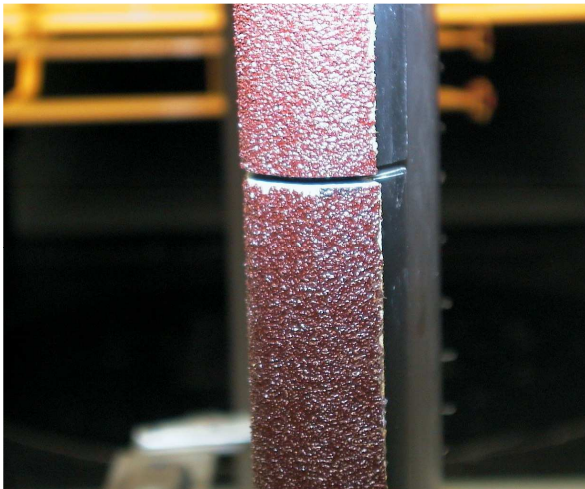

Fig. 4. Artificial roughened ice shape with pressure 'canyon'

2.3 Instrumentation

DNW was responsible for all data acquisition activities during the subject test. The model static pressures were measured by means of 1 PSI (6.9 kPa) pressure transducers using a HyScan pressure scanning system. This system also measures the pressures originating from the 4-fold wake rake. The wake rake pressures were also read out by a water multi manometer to be able to quickly center the wake rake to the wake. The wake rake was located at one chord length downstream of the flap trailing edge.

The tunnel reference data were measured by the standard DNW-LST wind tunnel reference measurement system.
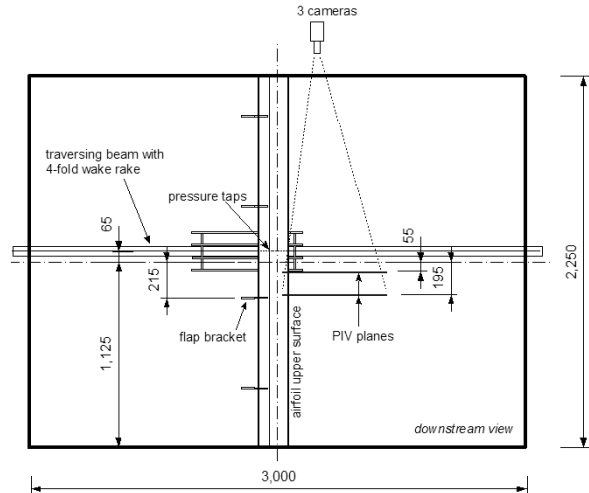

Fig. 5. Test set-up

Two double pulse Nd:YAG – lasers with 2 x 230 mJ pulse energy were mounted to the side of the wind tunnel, as part of the PIV system. A light sheet optic consisting of beam splitters and cylindrical lenses projected a single light sheet 6 mm thick and perpendicular to the spanwise direction on the model upper side. This allowed measurement of the U and V-velocity component in a spanwise section.

The basic spanwise position of the PIV laser plane was located 195 mm below the model center section, figure 5. In one test run the laser plane was moved up to 55 mm below the center section to get insight in possible spanwise variation of the flow and possible disturbance of the flow over the flap top surface by the flap mounting bracket on the lower surface (which turned out to be not the case).

3 PCO double-shutter, 1 Megapixel (1280 x 1024 pixel) cameras were mounted on the top turn table of the test section viewing through a hole in the tunnel ceiling. The gross field of view of the cameras is shown in figure 6. There was a small overlap in fields of view. As the cameras were mounted on the turn table, the field of view relative to the airfoil remained the same for all angles of attack. At each angle of attack 1000 pairs of images were taken, with an acquisition rate of roughly 3 Hz.

Seeding was provided by a seeding generator using Di-Ethyl-Hexyl Sebacate (DEHS) and entered the tunnel circuit downstream of the test section through the breather doors.
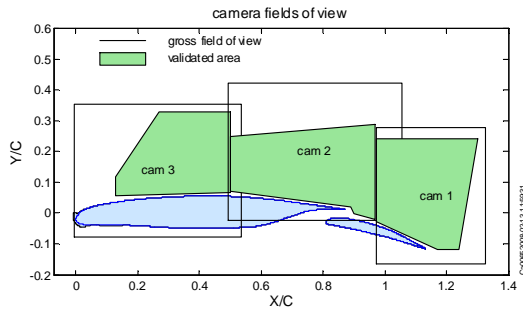
Fig. 6. Test set-up

2.4 Data processing

Initial processing of the PIV data was done by DNW using the standard PIV cross correlation method. For this purpose, the images are divided into 32-by-32- pixel interrogation areas, with an overlap of 50%. The physical size of these areas equals 10x10 mm^2. Areas in the field that were not trusted were masked and excluded already from the initial data processing. This concerned the area close to the airfoil surface were light reflections from the model were dominant and the region closely behind the ice ledge where much light scatter occurred due to the sandpaper on the ice ledge and the aluminium tape used to fix the ice shape.

2.5 Data correction

DNW having completed the standard data correlation of the PIV images, data were further refined by NLR by applying a number of corrections. The most important corrections will be described here.

Vertical shift

A vertical shift in the test data was observed between several test runs. These shift were of the order of a few %C. The positions in the flow field are calibrated using a grid drawn on a board that is positioned at the light sheet location and subsequently pictured by the PIV-camera's. This calibration is done without wind. Bending of the model under wind loads may be thought of as a reason for causing this shift. However, the amount of bending at the wing mid-span position is estimated to be around 0.6

mm at maximum lift, which is much smaller than the deviations found. The most likely cause seems to be a small change in camera-alignment related to the aerodynamic loading on the model, possibly by a small deformation of the wind tunnel turn table. For a shift of 10 mm in Y, the camera needs to rotate only 0.3°. For the final results the data obtained by the centre camera (C2) for each run have been matched to data obtained by a boundary layer rake during the test campaign of 1994 [1]. Vertical shifts to the data of the other cameras (C1, C3) have subsequently been applied to put the velocity profiles in the overlap regions for each camera on top of each other between the test runs. The required vertical shifts depended on the incidence and were found to be 2.5%C at maximum.

Large rms values

Obvious deviations in average flow velocity and/or high r.m.s. levels were observed in relatively large regions either close to the laser light sheet boundaries, close to the camera field of view edges and close to the model surface. This was most probably caused by deteriorating correlation due to reduced laser light sheet intensity or due to camera limitations. The following measures were taken to assure data quality: first the edges of the field of view that show generally deteriorated results have been cut off leaving an initial guess of the 'valid' area per camera. Secondly, the 'time' signals at a number of critical positions inside the validated areas were inspected manually to invalidate longer time stretches of measurement data that apparently suffered under bad correlations, possibly due to longer-duration light sheet or seeding deterioration. This was used to further limit the validated areas, to the areas as shown in figure 6.

Individual samples

Each frame within the remaining signal parts was post processed to detect remaining bad correlations on individual samples. The detection of these correlations used a 3σ-approach:

$$\left| \langle U_{i,j} \rangle - U_{i,j} \right| > 3\,\sigma_U\, U_{i,j} \qquad \text{and/or:}$$

$$\left| \langle V_{i,j} \rangle - V_{i,j} \right| > 3\,\sigma_V\, V_{i,j}$$

for each pixel, where σ denotes the r.m.s. value of the velocity. $U_{i,j}$ is the time-mean axial velocity at pixel i,j and $\langle U_{i,j} \rangle$ the value of the axial velocity component at a given time-instant and idem for the vertical velocity component $V_{i,j}$. If such a sample was found the local velocity vector was replaced by the average of the instantaneous, valid velocities in the 8 surrounding pixels. In case there are no valid surrounding pixels, the time mean velocity at that position is taken instead. It was verified that choosing a validation crest factor of 3 does not affect 'healthy' time signals too much, even if they have a somewhat skewed probability density distribution. It should be kept in mind however that any method used to remove outliers has a subjective element in itself and therefore is inherently dangerous. Choosing a crest factor of 3 gives a good compromise between desired correction of outliers and undesired rejection of valid points. In general the present choice of the multiplier leads to a correction of around 1 to 2% of the pixels.

The corrected data were processed to average velocity fields, Reynolds stresses, divergence and vorticity.

2.6 Error estimates

The error magnitudes have been estimated. A summary is shown in the table below. The position errors are deduced from the Y-shifts to obtain velocity field overlap. Although the errors in X-direction can not be determined in this way within a reasonable accuracy, it is assumed that the position errors are independent of the direction in a plane perpendicular to the span and therefore are taken equal in X- and Y-direction.

X/C, Y/C	±0.008
G/G_{ref}, U/G_{ref}, V/G_{ref}	±0.015
u'/G_{ref}, v'/G_{ref}	±0.01
$\overline{uv}/G_{ref}^2$	±0.015
C_p	±0.005
C_l	±0.06
C_d	±0.002
C_m	±0.02

Table. Error estimates

The errors in average velocities (G, U and V) have been determined from statistical analysis of the time-signals and are typically of the order of 1 to 1.5%, depending on the local turbulence levels. The larger errors occur close to the airfoil surface. The errors in the turbulence quantities themselves have been determined in the same manner. These errors are estimated to be around ±0.01 in u'/Gref and v'/Gref. For the turbulent shear stress the value is around ±0.015.

The errors in the wing force coefficients have been taken equal to those given in [1]. The uncertainty in Cl and Cm is relatively large due to the inaccuracy of the pressures in the ice shape region.

3 Results

The initial test runs were performed on a *clean* model, in order to verify flow 2-dimensionality using flow visualization. Subsequently the settings of the wall blowing slots were verified and tests were done with the ice shape attached. These tests focused on optimizing the 2-dimensionality for this configuration. This resulted in removing about 50 mm of ice ledge next to the tunnel walls in order to allow for a more effective operation of the wall blowing system. A detailed comparison with the pressure measurements of 1994 then resulted in the final selection of incidence settings used for the present test. The test was completed with the PIV runs.

All tests were performed at a Reynolds number Re = 3×10^6, based on the reference wing chord C. The corresponding tunnel reference flow velocity amounted to about 70 m/s or Ma = 0.2. The basic incidences at which the measurements were done ranged from pre-stall to post-stall: α=0.5°, 3.5°, 4.5°, 5.5°, 6.5° and 8.5°.

3.1 Flow visualisation

The flow on the airfoil was visualized by means of tufts on the model upper surface. The general tuft patterns show an attached flow at α=0.5° with some tuft-unsteadiness. At α above

3.5° flow separation is visible behind the ice-shape up to roughly 30%C, increasing to about 40-45%C at α=4.5°. At α=5.5° the flow is fully separated on the main component but the flap remains attached at all angles of attack (the last two rows of tufts in figure 7).

Fig. 7. Tuft pattern at α=5.5°

The same holds for 6.5° and 8.5° but at these incidences there are increasing non 2-dimensional features. Especially at 8.5° there is a small region just above the pressure section were the tufts indicate an angled but seemingly non-separated flow. This pattern is unsteady: it sometimes 'flip-flops' such that the pattern changes symmetrical with respect to the pressure tap section from above the pressure section to below the pressure tap section. The related typical flip-flop period is of the order of a few seconds at α=8.5°, but much faster (a few Hz) at α=6.5°. This behavior appeared not to be related to the 'pressure tap canyon' in the ice shape as it occurred also when the canyon was closed by taping it off. It was remarkable that the PIV 'time traces' did not show any indication of a flip-flop, not even at the points closest to the airfoil surface. So, the unsteadiness seems to be confined to a thin layer close to the surface of the airfoil.

The tuft pattern on the flap shows that the flow at the flap is attached at all tested incidences, even at α=8.5°, although the tufts close to the flap trailing edge are fluctuating much more, hence show signs of incipient separation. The PIV data at this incidence also show signs of intermittent separation on the flap at this incidence.
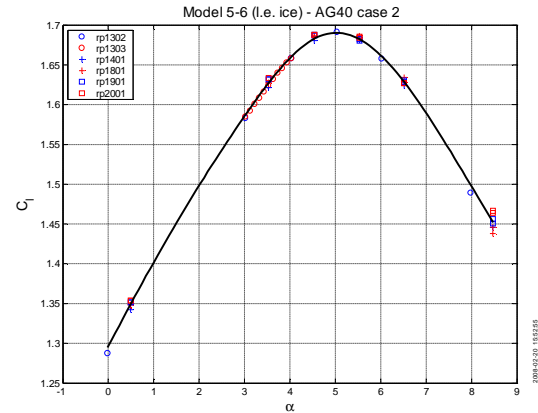
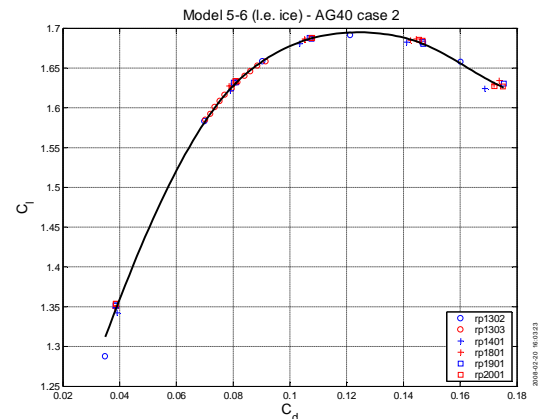## 3.2 Airfoil characteristics

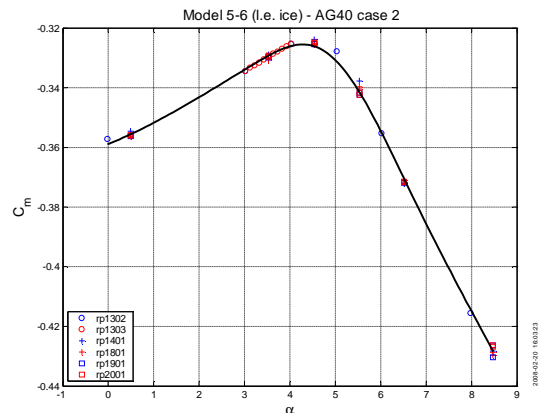Fig. 8. Lift (iced)

Fig. 9. Drag (iced)

Fig. 10. Pitching moment (iced)

C_l and C_m were determined from the pressure distributions. As the leading edge pressures are inaccurate, due to the presence of

the ice shape, these values – especially C_m - must be considered with care. In the 1994 tests [1], C_l was determined both from the tunnel wall pressures (the more accurate one) and from the model pressures. It was found that $C_{l,max}$ from the tunnel wall pressures was about 0.08 higher, and at $\alpha=0°$ the difference amounted to about 0.01. This is mainly explained by the fact that the (suction) pressures in the ice canyon are too low.

Fig. 11. Pressure distributions at α = 0.5°, 4.5° and 6.5°. (iced)

The C_l, C_d and C_m-curves from the present test are shown in figure 8 to 10. C_d at $\alpha=8.5°$ (the curve end point) is uncertain and probably too low as the wake at this incidence is too wide for the wake rake due to the massive separation. As a number of different runs are shown in these figures, they also give an idea about the good repeatability of the present measurements even at and post stall.

3.3 Pressure distributions

The pressure distributions at $\alpha=0.5°$, 4.5° and 6.5° as measured at the start and the end of the PIV-measurements are shown in figure 11. The main component and flap pressures are drawn in one graph. The flap pressures are located at X/C>0.8 and the main component pressures at X/C<0.87. So, a small overlap is present between both distributions. There is a 5 minute time difference between the 2 data sets, corresponding to the time required for taking the 1000 PIV frames. An excellent reproducibility is shown, indicating that the flow stability is good. The pressure distributions on the main component show the effect of flow separation at $\alpha=6.5°$, resulting in a decrease of the leading edge pressure peak and a decrease in pressure gradient on the suction side.

The pressure distribution on the flap shows that the flow is unseparated, as was also shown by the tufts, and remains nearly unchanged between 0.5° and 6.5°. At $\alpha=6.5°$ it is seen that the flap starts taking more load due to the severe separation on the main component. At $\alpha=8.5°$ the flap is at incipient separation. However, also at 6.5° the flap shows an increase in dumping velocity already.

3.4. PIV results

PIV measurements have been performed in 3 separate test runs. Each run covered the same series of incidences as mentioned before. Between the runs small modifications to the optical set-up were performed. Some results at $\alpha=6.5°$ will be shown here, flow features at other angles of attack will only be described.
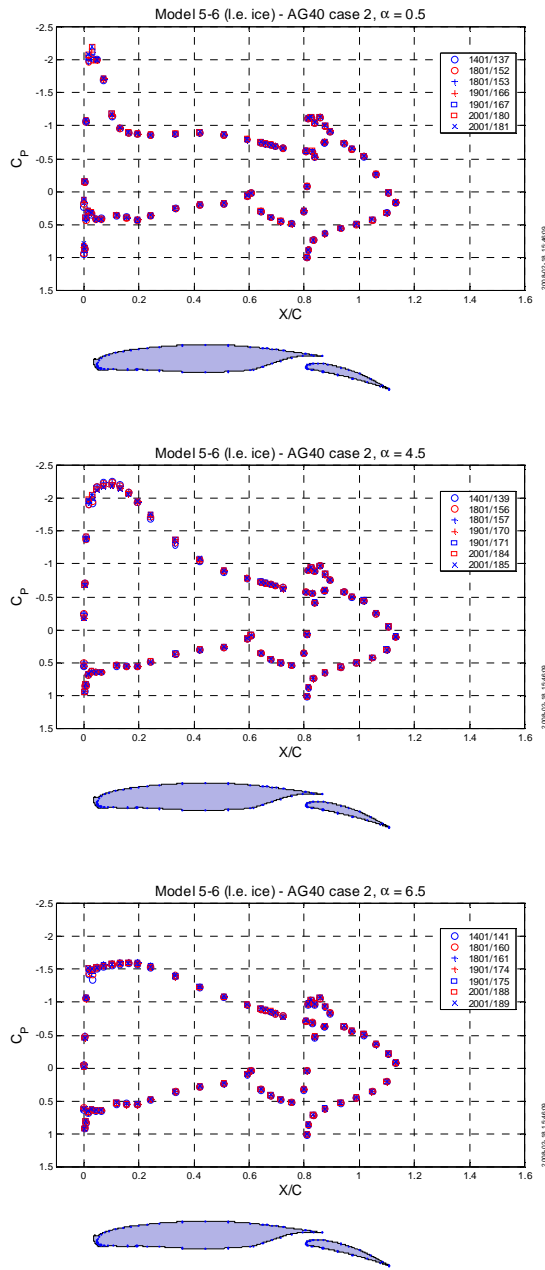
Instantaneous flow field

To get some insight into the flow fields, figures 12 and 13 show an instantaneous flow field at α=6.5°. As the 3 cameras are synchronized taking the frames, the individual pictures of the cameras can be combined into one large full-chord picture of the instantaneous flow field. To get a better visualisation of the flow features, figure 12 shows the difference of the individual velocity vectors relative to the *local* average $G_{i,j}$ instead of the flow vectors themselves, i.e. $\langle G_{i,j}\rangle$-$G_{i,j}$.
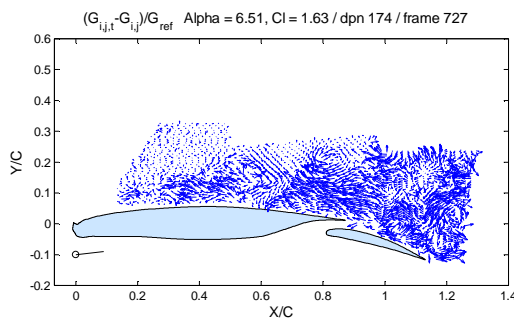
Fig. 12. Instantaneous velocity fluctuation α=6.5°
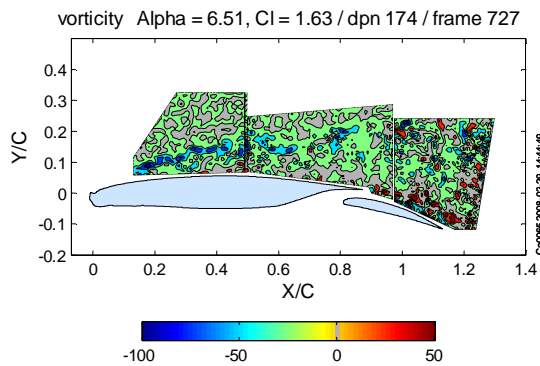
Fig. 13. Instantaneous vorticity distribution, α=6.5°

Significant separation can be observed at α=6.5°. The separating shear layer is leaving the ice ledge roughly under the same angle as the incoming flow (reference flow direction indicated by the small 'tuft' in the lower left corner of figure 12). The shear layer was still fairly well organised at α=4.5°, but at α=6.5° the instability has increased considerably.

It would be interesting to further investigate this flow using e.g. proper orthogonal decomposition (DOP) to see whether there coherent large-scale flow features in this shear layer [2], [3], [4]. It is clear that the flow exhibits a large variety in length scales at this post-stall incidence. The largest eddies appear to have sizes of the order of 10% chord. And, as is seen from figure 13, most unsteady activity is found at the shear layer edge as may be expected.

Time average flow field

In figures 14 to 19 time-average flow field quantities are shown. In figure 14 the large thickness of the viscous region is visible. At α=0.5° the viscous region behind the ice shape in the leading edge region is thin and located below the PIV validated area, closely above the surface. At $C_{l,max}$ and above (α≥5.5°) a large separated area is found behind the ice shape.
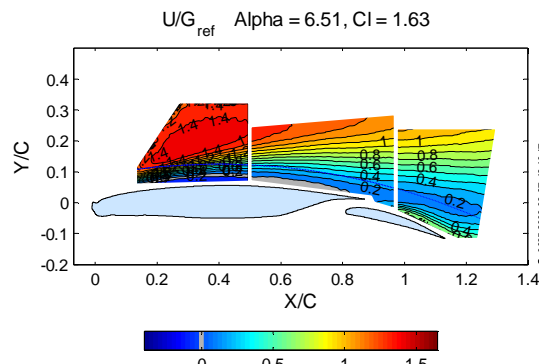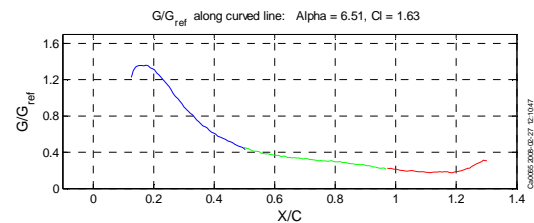

Fig. 14. Mean axial velocity U/G_{ref}, α=6.5°

Fig. 15. Distribution velocity magnitude G/G_{ref} along arc in field, α=6.5°

At α=6.5° a region with backflow (U<0) is just visible in the axial mean velocity distribution, close to the airfoil surface. The grey band indicates the location where U ≈ 0. At 8.5° this region also stretches out over the flap, although the flap flow itself is still just attached.

The dashed line shows the arc in the field along which the distribution of the total velocity vector magnitude $G = \sqrt{U^2 + V^2}$ is determined, as shown in figure 15. Different colors in this distribution are obtained by different cameras.

The shear layer itself can be observed very well in the vorticity distribution, figure 16. The vorticity level is defined as:

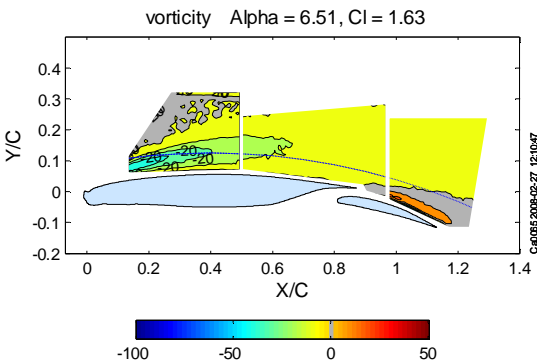$$\gamma = \frac{C}{G_{ref}}\left(\frac{\partial V}{\partial X} - \frac{\partial U}{\partial Y}\right)$$

Fig. 16. Vorticity, α=6.5°

The shear layer is departing from the airfoil surface at an increasing angle with increasing angles of attack. At α=6.5° the shear layer is still somewhat following the upper surface contour, but this is no longer the case at 8.5°. At incidences of 4.5° and less reattachment occurs. This is below $C_{l,max}$. At 5.5° reattachment is no longer visible in the PIV-results. These results correspond to the flow visualization observations.

For a two-dimensional flow the spanwise gradients should be zero. Therefore this gradient has been determined, using the continuity equation:

$$-\frac{\partial W}{\partial Z} = \frac{\partial U}{\partial X} + \frac{\partial V}{\partial Y}$$

The value of the spanwise gradient $\partial W/\partial Z$ remains small, typically being one order of

magnitude smaller than the vorticity if made dimensionless in the same way as γ. Taking into account the inaccuracies in determining derivatives from experimental data this gives no indication that the flow is not 2-dimensional.

For each incidence 1000 velocity field images have been taken. This offers the possibility to get an impression on the turbulence quantities. Ideally, more samples would be required to reduce the scatter and inaccuracy in the turbulent quantities. Nevertheless, fair results were obtained as can be seen below.

Figure 17 shows that the axial turbulence intensity increases strongly in the separating shear layer. This is associated with the large local flow gradients. Maximum levels amount to around 50% in the forward part of the shear layer. Above the flap trailing edge it seems that turbulence levels are lower. In an absolute sense this is true as the turbulence intensities shown have been made dimensionless with the reference flow velocity G_{ref}. However if the local (low) mean flow velocities would have been taken as a reference, it appears that also in this region the local turbulence intensities are high which is not surprisingly as there is a significant pressure loading on the main component wake above the flap.

The turbulence intensities in vertical direction are much smaller as figure 18 shows. Roughly the maximum values are about 1/3rd of the axial turbulence intensity, which is related directly to the dominant velocity gradients being in vertical direction, thus promoting axial turbulence intensity.
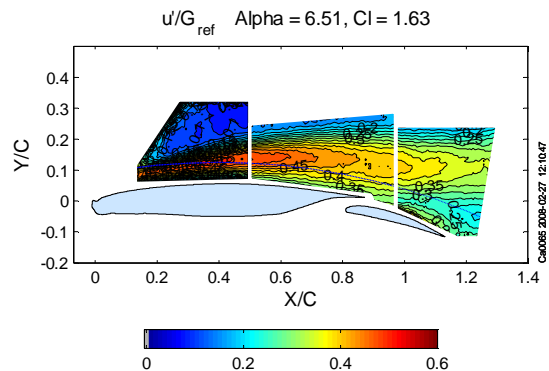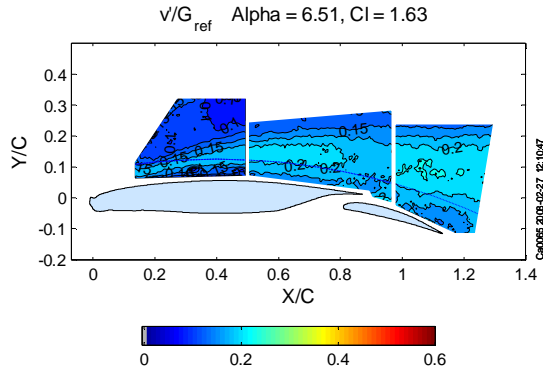

Fig. 17. Axial turbulence intensity u'/G_{ref} , α=6.5°

9

Fig. 18. Vertical turbulence intensity v'/G_{ref}, α=6.5°

Finally, the turbulent shear stress can be inspected in figure 19, showing the shear stress correlation coefficient $\overline{uv}/(u'v')$. At incidences below 8.5° the maximum correlation coefficient in the shear layer amounts to about 0.5, a fairly normal value. At 8.5° the maximum only reaches a value around 0.4. Also, the maximum shear layer shear stress values occur at α=6.5°, whereas the maximum shear values found at α=8.5° are lower. So, apparently the widening of the shear layer at 8.5° leads to reduction in shear stress and a loss in correlation between the u- and v-fluctuation.
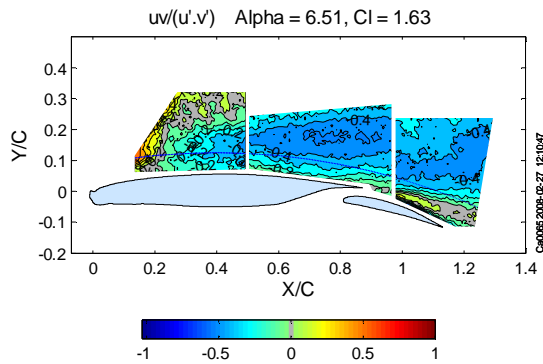

Fig. 19. Shear stress correlation coefficient $\overline{u.v}/(u'.v')$, α=6.5°

4 Conclusions

PIV flow field measurements have been performed in DNW-LST on the upper surface of a 2-dimensional high lift, single flap, airliner airfoil equipped with a leading edge, intermediate type of ice shape. The measurements were done at incidences below and above that for maximum lift at angles of attack between 0.5° and 8.5°. As the measurements were done using three synchronized cameras, instantaneous flow pictures have been obtained of almost the full upper surface flow.

An extensive data base with flow field data has become available for validation purposes of CFD tools.

PIV data post processing tools have been developed by NLR for preliminary data analysis purposes.

The experimental data show that the separated flow behind the ice shape reattaches to the airfoil surface at angles of attack up to and including 4.5°, i.e. just below the maximum lift incidence. This corresponds to flow visualization results. Past maximum lift, α=5.5°, there is a massive separation and reverse flow region on the upper surface.

References

[1] Reinders W. *Data paper of the effect of in-flight icing on the 2D high lift model 5-6 in the low speed wind tunnel LST.* NLR CR 94551, December 1994.

[2] Van Oudheusden B., Scarano F., Van Hinsberg N.P., Watt D.W. Phase-resolved characterization of vortex shedding in the near wake of a square-section cylinder at incidence. *Exp.in Fluids*, Vol. 39, pp 86-98, 2005.

[3] Berkooz G., Holmes P., Lumley J.L. The proper orthogonal decomposition in the analysis of turbulent flows. *Ann. Rev. Fluid Mech.*, Vol.25, pp.539-575, 1993.

[4] Sirovich L. Turbulence and the dynamics of coherent structures, *Quart. Appl. Math.*, Vol.45, pp.561-590, 1987.

Copyright Statement